Reaction Chemistry & Engineering

ROYAL SOCIETY OF CHEMISTRY

PAPER

View Article Online
View Journal | View Issue

Cite this: *React. Chem. Eng.*, 2024, **9**, 1762

TiO_2 nanopowder and nanofilm catalysts in the disinfection and mineralization of *S. aureus* with solar-simulated radiation†

Raed Shqier,[a] Ahed Zyoud,[a] Muath H. S. Helal,*[b] Heba Nassar,[a] Raed Alkowni,[a] Mohyeddin Assali,[c] Shaher Zyoud,[d] Naser Qamhieh,[e] Abdul Razack Hajamohideen,[e] Shadi Sawalha,[f] Samer H. Zyoud[g] and Hikmat S. Hilal[a]

Water contamination with various microorganisms is life threatening. TiO_2 semiconductor nanoparticles have been widely described for bacterial inactivation. However, such a process may yield hazardous organic matter in water; complete bacterial mineralization is thus imperative. This study describes how anatase TiO_2 nanopowder, suspended in water, photocatalyzes the inactivation and complete mineralization of *Staphylococcus aureus* using UV radiation from simulated solar radiation. Total organic carbon (TOC) analysis confirms bacterial photo-mineralization. Bacterial mineralization is further evidenced by the appearance of ammonium ions in the treated water. In the dark, and under visible light using a cut-off filter, only a small fraction of bacteria is inactivated with no mineralization. Nanofilm catalysts are also examined in batch reaction systems. The film catalyst exhibits a higher photocatalytic efficiency with a turnover frequency of up to ~4.9×10^8 CFU g^{-1} min^{-1} compared to ~5.8×10^6 CFU g^{-1} min^{-1} of the nanopowder film counterparts. The powder catalyst lost up to 65% of its efficiency on reuse. This is due to catalyst lost mass during recovery by filtration. The film catalyst retains about 96% of its efficiency upon second reuse, showing its feasibility in application. Moreover, the film catalyst is useful in a continuous flow reaction system with an efficiency of 5.4×10^8 CFU g^{-1} min^{-1}, which is higher than that in the batch system, and no measurable efficiency loss in reuse. These results open the door to use the present photodegradation process in large-scale water purification processes.

Received 14th October 2023,
Accepted 5th March 2024

DOI: 10.1039/d3re00540b

rsc.li/reaction-engineering

1. Introduction

Water sources are subject to many types of hazardous pollutants, including chemical[1] and biological species.[2,3] Water remediation is thus necessary to eliminate various contaminants and microorganisms, especially from drinking water.[4] For this purpose, various methods are followed at the research and commercial level, including chlorination,[5] peroxidation,[6] UV irradiation,[7] reverse osmosis[8] and others.[9] Despite their effectiveness, such methods still suffer from a number of drawbacks. For example, water chlorination produces hazardous chlorinated hydrocarbon by-products in water.[10] Peroxidation, UV irradiation and reverse osmosis can be costly and non-feasible for use in rural areas with limited economic resources. New trends in research[11,12] are emerging where direct solar radiation is being used in water purification (from chemicals) and disinfection (from microorganisms). Metal oxide nanoparticles, such as those of ZnO and TiO_2, are commonly investigated for water purification. Such materials have been widely described in the photodegradation of aqueous chemical contaminants, such as dyes, halo-organics, phenols, and pesticides. The materials were also described to disinfect water from bacteria.[13,14] Nanoparticles of both ZnO and TiO_2 are known to inactivate both Gram-positive and Gram-negative bacteria

[a] *Faculty of Sciences, An-Najah National University, Nablus, P400, Palestine*
[b] *Department of Biomedical Sciences, Faculty of Medicine and Health Sciences, An-Najah National University, Nablus P400, Palestine.*
E-mail: muath.helal@najah.edu
[c] *Department of Pharmacy, Faculty of Medicine and Health Sciences, An-Najah National University, Nablus P400, Palestine*
[d] *Department of Civil Engineering & Sustainable Structures, Palestine Technical University (Kadoorie), Tulkarem P304, Palestine*
[e] *Department of Physics, United Arab Emirates University, P.O. Box 17551, Al Ain, United Arab Emirates*
[f] *Department of Chemical Engineering, Faculty of Engineering and Information Technology, An-Najah National University, Nablus P400, Palestine*
[g] *Department of Mathematics and Sciences, Ajman University, P.O. Box 346, Ajman, United Arab Emirates*

† Electronic supplementary information (ESI) available. See DOI: https://doi.org/10.1039/d3re00540b

in the dark and under irradiation. The mode of action of nanoparticles involves rupturing the bacterial cell wall, which causes the organic content of the cell to leach out, thus leading to inactivation.

Despite the high efficiency of metal oxide nanoparticles in bacterial growth inactivation and water disinfection, the process has not been fully investigated in literature. In the case of high bacterial concentrations, high amounts of organic matter may leach out into water. Such organic matter itself is hazardous. Typically, the upper limit for allowed organic content in water is 5 ppm. In some cases, the organic matter leaching out after bacterial inactivation reached ~40 ppm or higher.[15] This value is too high and is a cause for concern. Moreover, the fate of inactivated bacteria has not been described enough in the literature. Attention has been mostly paid to bacterial growth inhibition and inactivation.

In our search for practical processes to completely inactivate and mineralize bacteria from water, we have reported on using suspended ZnO nanoparticles as photocatalyst systems under direct solar light. The choice for ZnO particles is due to their reported efficiency in rapturing bacterial cell walls.[15,16] With a band gap value of ~3.2 eV, the particles can be excited by photons with a wavelength of 387 nm or shorter. Therefore, the ZnO particles were sensitized by other dyes to function in the visible range. Such method may not be practical for use in stand-alone purification stations in remote areas, for more than one reason. The ZnO particles are known to partly dissolve in water at relatively low pH values. The dye sensitizer may itself be degraded during photodegradation. Moreover, the suspended ZnO nanoparticles cause technical difficulty in separation.

TiO_2 nanoparticles have been widely described in bacterial inhibition and inactivation. De Dicastillo *et al.* reviewed how TiO_2 may affect various types of bacteria.[17] The report described how the TiO_2 particles may affect the bacteria in the dark and under irradiation. The effects on the cell walls, the cell membranes, the DNA and other bacterial processes were described. Inactivation and killing of bacteria by TiO_2 under radiation[18] and by combination with antibiotics[19] were described. TiO_2 particles mixed with other species such as Si have been recently described as antibacterial photocatalysts.[20] Photo-inactivation of various types of bacteria, catalyzed by TiO_2/Si films, was also described.[21] Despite the vast literature on TiO_2 effects on bacteria, the studies were focused on bacterial death, inactivation, and inhibition, with no reference to what happens after that. What happens to organic materials, which leach out of the inactivated bacteria, has not been described to our knowledge.

Herein, TiO_2 nanoparticles will be employed in bacterial inactivation and complete mineralization under solar-simulated light for the first time. As TiO_2 particles have a band gap of ~3.2 eV, they need photons of ~300 nm for excitation. Fortunately, such photons are available in solar-simulated radiation, although at relatively low fractions of ~5%.[22] The ability of TiO_2 nanoparticles to achieve the objectives will be assessed here. The Gram-positive bacterium, *Staphylococcus aureus* (*S. aureus*), has been chosen here due to its special features. The bacteria have thick peptidoglycan walls, which make them resistant to radiation. The bacteria are well known for their roles in infectious diseases in many places of the human body,[23] including medical implants.[24] *S. aureus* can live in a wide range of temperatures from −18–40 °C.[25] *S. aureus* may also grow in a wide pH range from 4.0–9.8, preferably at ~7.[25,26]

The present study will thus answer the following questions: can TiO_2 nanoparticles photocatalyze the complete mineralization of aqueous *S. aureus* with solar-simulated radiation? What happens to the organic stuff that leaches out of the raptured bacteria? To recover the TiO_2 nanoparticles for further reuse, can the particles be coated onto glass surfaces and used as film photocatalysts? Will the coated films be able to catalyze the bacterial mineralization when used in continuous flow processes? All such questions will be answered here based on the following assumptions. Firstly, bacteria can be inactivated by TiO_2 particles as described above. On the other hand, the particles are known to photocatalyze organic contaminant mineralization in water, as reported earlier.[27–29] Secondly, the TiO_2 films should exhibit higher catalytic performance than the powder form because the powder particles, at the surface of the reaction mixture, may screen incident radiation from reaching other catalyst sites inside the bulk reaction mixture. Such difficulties can be overcome by film catalysis, as the catalyst sites at the catalyst film will be exposed to incident radiation without much screening. In continuous flow reactions, the bacterial solution can be passed atop the catalyst film particles at suitable flow rates to allow enough time for complete bacterial mineralization. These assumptions will be tested here, and the research questions will be answered here for the first time. Literature mechanisms will be used to rationalize the achieved findings.

2. Materials and methods

2.1. Starting materials

Chemically pure materials, including organic solvents, acids and bases, were purchased from Sigma-Aldrich, Merck or Alfa Chem. High-purity anatase titanium oxide (TiO_2) powder, with particle sizes of ~25 nm and specific surface area of ~45–55 $m^2\ g^{-1}$, was purchased from Sigma-Aldrich 232033 (MDL MFCD00011269). The anatase powder was further characterized as described below. Nutrient broth was purchased from Hi Media Lab Pvt. Ltd, India, and the agar was from Sparks, Becton, Dickinson USA.

The Gram-positive (G+) *S. aureus* bacteria were generously donated by the Medical Science Laboratory of An-Najah National University. The bacteria have been isolated from clinical samples. All safety standards have been strictly followed, including reference to materials safety data sheets for all chemicals. Standard protocols have been strictly followed under direct expert supervisions, while performing

the bacterial culturing, measurement and processing. The present study does not involve any experiments on any humans, animals, insects or plants.

2.2. Equipment

A Labo Med, Inc. 1601 spectrophotometer was used to prepare the bacterial solutions. Solid-state electronic absorption was measured for the anatase powder suspended in water on a Shimadzu UV-1601 spectrometer using water as the baseline. A Perkin Elmer SL50B spectrophotometer was used to determine the solid-state photoluminescence (PL) spectra for the TiO_2 layer at an excitation wavelength of 300 nm.

Solar-simulated radiation was made using an HLX64657 EVC (250 W) halogen-tungsten lamp. The intensity at the reaction mixture surface was fixed at 100 000 Lux (0.136 W cm^{-2}) in all experiments by controlling the distance above the reaction mixture.

A Philips XRD-XPERT PRO diffractometer Cu K (source λ = 1.45 Å), at UAE University-Al-Ain, was used to measure the XRD patterns. The SEM micrographs have been measured on a Jeol Model JSM-6700F at UAE University, Al-Ain. The total organic carbon (TOC) in the treated bacterial solutions was measured in triplicate on a SHIMADZU analyzer Model TOC-L CSH/CSN at Palestine Technical University, Tulkarm, Palestine. The TOC method determines all organic carbon materials in the reaction mixture, including the remaining bacteria (dead or alive), remaining broth and all resulting organic stuff. The atomic force microscope (AFM) image of the titanium dioxide thin film was measured on a CoreAFM (Nanosurf, Switzerland). The tapping mode was used with a force constant of 5 N m^{-1} for the probe at a resonance frequency of 150 kHz. Gwyddion software was used to analyze the images.

2.3. TiO_2 film preparation

TiO_2 films were prepared by the drop-casting method on high-quality microscopic glass slides (7.5 cm × 2.5 cm). Prior to use, the glass slides were cleaned with deionized water, acetone, deionized water, and HCl, then rinsed again with deionized water and dried.

Films were prepared separately using identical procedures. The anatase TiO_2 powder was thoroughly mixed with acetyl acetone, Triton X-100 and water (10 : 20 : 30 : 40 by mass). The mixture was then sonicated (10 min) at room temperature to create a slurry. Then, using the drop-casting technique, the slurry was dropped onto a heated rotating glass substrate. The films were sintered (h) at 300 °C for 1 h. The temperature was just enough to give stable adherence of the anatase TiO_2 particles onto the glass surface. It does not cause any phase change in the anatase, which is well-documented.[30] TiO_2 retains its anatase phase when heated at temperatures much higher than 300 °C.[31,32]

2.4. Bacterial solution preparations

The *S. aureus* (Gram-negative bacteria), isolated from clinical samples, was generously donated by the Medical Science laboratory of An-Najah N. University. Agar nutrients were prepared using the manufacturer instruction protocols, and poured onto pre-sterilized dishes to allow for bacterial counting. Nutrient broth was been prepared using the manufacturer protocols. The broth was poured in 5 mL pre-sterilized test tubes.

A standard McFarland solution was prepared from stock solutions of $BaCl_2{\cdot}2H_2O$ (0.96 N, 0.175 mass/V) and of H_2SO_4 (0.36 N, 1.0 V/V). Aliquots of $BaCl_2$ (0.05 mL) and H_2SO_4 (9.95 mL) were mixed together. The measured optical density (at λ = 625 nm) for the solution was determined in the range of. 0.08–0.10. The measured optical density resembles the optical density for a bacterial concentration of 1.5×10^8 CFU mL^{-1} in the powder catalyst reactions.

A 0.9% (by mass) normal saline was prepared by dissolving NaCl (4.5 g) in 500 mL of deionized water. The initial pH was controlled as desired by dropwise addition of HCl (0.25 M) or NaOH (0.25 M) solutions. The inocula of bacteria were prepared by inoculating a bacterial loop-full inside the sterilized broth (50 mL), followed by a 7 h incubation at 37 °C. The concentration of *S. aureus* in the original broth was determined as 1.5×10^8 CFU mL^{-1} (equivalent to 0.5 McFarland concentration) in the powder catalyst runs. Cell suspensions for photodegradation study were prepared by dilution of aliquots (167 μL) from the original broth with deionized water (50 mL) at controlled pH values of 4.5, 7.4 and 9.0 to reach the $\sim 5 \times 10^5$ CFU mL^{-1} concentration. Unless otherwise stated, the default pH value 7.4 was used here. The default initial bacterial amount used in the powder catalyst experiments is a 50 mL solution of $1 \times 10^6 \pm 5000$ CFU mL^{-1}. The default initial bacterial amount in the film experiments is 100 mL solution of $6.5 \times 10^6 \pm 5000$ CFU mL^{-1}. The bacteria remaining under experimental conditions were microscopically measured by plate counting method, as described in standard procedures.[33] Fig. S1† shows a sample image of the bacteria before and after treatment.

2.5. Photodegradation experiments

Control and confirmation experiments were performed. In some experiments, bacterial solutions were exposed to radiation in the absence of any catalysts. In other experiments, the medium and broth solutions were tested under photocatalytic treatment. In photocatalytic experiments, bacterial and medium solutions were exposed to radiation in the presence of the catalyst. Dark experiments were also performed for comparison.

To determine which solar-simulated radiation region is active in the photocatalytic process here, a control experiment with a cut-off filter (that excludes wavelengths of 400 nm or shorter) was conducted. Therefore, bacterial solutions were exposed to solar-simulated radiation with and

without the cut-off filter that removes radiation at wavelengths shorter than 400 nm. Typically, solar-simulated radiation contains up to 5% UV photons with a wavelength of 400 nm or shorter.

Powder photocatalytic experiments were performed under air inside a pre-sterilized 100 mL (5 cm in diameter, gross area 19.6 cm^2) glass beaker thermostated by a water bath at ~25 ± 2 °C. Fig. S2† describes the photocatalytic experiments. Typically, bacterial growth is higher at 37 °C,[34] but natural water temperatures are lower than 30 °C. Therefore, the room temperature 25 ± 2 °C was used here for practical purposes. Bacterial diluted suspensions (50 mL of nominal 1×10^6 CFU mL^{-1} concentrations) were used in the degradation study. The TiO_2 powder (0.1 g) was suspended in the bacterial mixture with gentle stirring.

In both batch and continuous flow film catalyst systems, experiments were conducted inside Pyrex 500 mL beakers, (with ~9 cm diameter) and thermostated by a water bath at 25 ± 2 °C. Two slides of the film catalyst were placed, side by side, at the beaker bottom with face up. The total anatase mass in the two films is ~2–4.8 × 10^{-3} g with a total gross area 37.5 cm^2. The film thickness is 0.4 μm, as described below. In batch experiments, the bacterial solution (100 mL) was allowed to freely cover the film surface at a solution depth of ~1.6 cm in batch experiments. In continuous flow experiments, bacterial solutions (100 mL) were allowed to flow over catalyst films at a solution depth of ~0.5 cm over a period of 3 h, at a flow rate of ~0.56 mL min^{-1}.

The reaction mixtures were irradiated with the solar-simulated radiations at a measured intensity of 0.136 W cm^{-2} for a given time. The remaining bacteria numbers inside the reaction mixtures were measured by the spread-plate method. Aliquots (1.0 mL) were taken from the suspension, and diluted with sterile normal saline solution (9.0 mL, 0.9% NaCl by mass). Dilutions were successively made by standard methods. Samples (0.1 mL) from each dilution were uniformly spread on the plates and incubated at 37 °C for 24 h. For each dilution, three plates were used with three separate measurements. The dilution plates involving colonies of 30–300 were only considered, and the average bacterial colony numbers were taken. Initial and final bacterial concentrations were calculated. Bacterial loss percentage was calculated using eqn (1):

$$\text{Bacterial loss (\%)} = \frac{\left(\left(\text{Initial Bacterial CFU ml}^{-1}\right) - \left(\text{Final Bacterial CFU ml}^{-1}\right)\right)}{\left(\text{Initial Bacterial CFU ml}^{-1}\right)} \times 100\% \quad (1)$$

Catalyst recovery experiments were performed. The powder catalyst was recovered by simple decantation. The process was tedious as the complete recovery of the catalyst sample was not possible, especially from bacterial mixtures. The recovered catalyst was washed, heat sterilized and dried for reuse. Only low fractions (~35%) of the original catalyst were recovered.

In film catalyst systems, recovery was made by isolating the films with a tong, and then washing and sterilizing before reuse. In both systems, the recovered catalyst was used in the same way as the fresh catalyst system, as described above.

To confirm the bacterial mineralization, TOC values were measured for the reaction mixtures (before and after treatment). Moreover, solution nitrogen ions were measured to see if bacteria were mineralized during photodegradation experiments. The nitrogen ions, in the forms of nitrate, nitrite and ammonium ions, were analyzed by standard methods.[35,36]

3. Results and discussions

3.1. Characterization results

The commercial anatase TiO_2 nanoparticles were characterized by various methods. The vendors' specific surface area (SSA of 45–55 m^2 g^{-1}) for the powder anatase was confirmed by the acetic-acid adsorption technique, as reported earlier.[37,38] The approximate SSA measured value is ~52 m^2 g^{-1}.

The electronic absorption spectrum (Fig. 1a) involves a broad peak in the range of 370–384 nm, with a number of peaks. Similarly, the photoluminescence spectrum, measured at 300 nm excitation wavelength (Fig. 1b), shows the maxima in the range of 370–384 nm. Similar behaviors were reported.[39,40] The spectra describe a number of transitions in the anatase. The peaks at 384 nm correspond to a band-to-band transition with a band-gap value of ~3.23 eV, which resembles reported values.[41] The band gap has also been confirmed by the Tauc method,[42] as described earlier,[43,44] and the value is approximately 3.23 eV. The spectra thus confirm the dominant anatase phase in the used commercial TiO_2 powder here. The peaks at 417 nm are due to rutile impurity, as described by the vendor.

The surface morphology for the powder anatase TiO_2 was studied by SEM (Fig. 2). Small crystallites of approximate ~20 nm in size can be observed. The crystallites exist inside non-uniform agglomerates of various sizes of up to 400 nm. The agglomerates themselves exist in non-uniform large lumps of up to 1000 nm dimensions.

The XRD pattern was measured for the anatase powder, as shown in Fig. 3. The reflections (101), (103), (004), (112), (200) and (204) can be observed at 2θ = 27, 37, 38, 39, 48 and 63°, respectively. The pattern is typical for the anatase TiO_2 nanoparticle described earlier in JPCDS # 21-1272 and earlier reports.[45] Based on the ICDD card # 01-076-0317, the reflections at 2θ = 54, 57, 68 and 72° are due to the

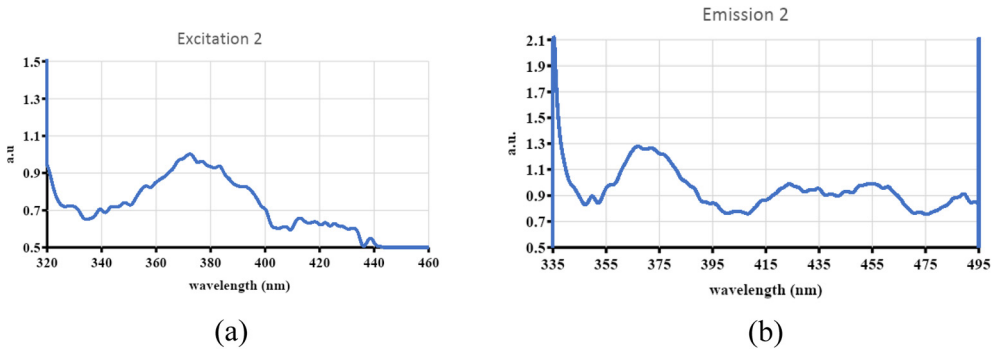

Fig. 1 Solid-state spectra for the anatase powder. (a) Electronic absorption spectra measured for a suspension of 0.1 g TiO_2 in 50 mL water, and (b) photoluminescence spectra measured for the solid TiO_2 film under 300 nm excitation wavelength. All measurements were carried out at room temperature.

minor rutile TiO_2 phase described by the vendor to be ~5%.

By Scherrer relation (eqn (2)[46]), using the reflections (101) and (112), the average crystallite size is ~35 nm. The value is larger than that reported by the vendor company (~20 nm).

$$D_{(hkl)} = \frac{K\lambda}{B_{(hkl)}}\cos(\theta), \quad (2)$$

where $D_{(hkl)}$ is the crystallite size based on the reflection plane (hkl), K is the shape constant ~0.9, λ is the wavelength for incident X-rays, $B_{(hkl)}$ is the width at half height maximum (FWHM) in radians, and θ is the Braggs' angle.

Together, the XRD and SEM results indicate the presence of smaller anatase TiO_2 crystallites inside larger agglomerates. Together with the spectral results, the diffraction results confirm the anatase nature for the commercial TiO_2 used here.

The prepared TiO_2 film has been characterized with atomic force microscopy (AFM). Fig. 4 shows the spherical-shaped TiO_2 agglomerates of an average of 200–400 nm in diameter. The measured film thickness is in the range of 0.300–0.500 μm. Based on AFM, the average film thickness is 0.4 μm. Knowing the density for anatase TiO_2 is 4.23 g cm^{-3}, the total TiO_2 mass on each slide (2.5 × 7.5 cm^2) is ~3.2 × 10^{-3} g.

3.2. Photocatalytic experiments

The ability of various anatase photocatalyst systems to inactivate and mineralize *S. aureus* was determined. The catalytic performance was measured in terms of bacterial loss%, as described in eqn (1). The relative catalyst efficiency was measured in terms of the turnover number (TN = lost bacteria per TiO_2 per g catalyst), turnover frequency (TF = TN min^{-1}) and quantum yield (QY = lost bacteria/UV incident photon per g cat). Each experiment was repeated 3 times using fresh samples of catalyst and bacterial solution, with error of ±10%. The average values of lost bacterial were calculated as shown below.

Cut-off experiments indicate that the TiO_2 particles exhibit photocatalytic behavior upon exposure to the UV region in the incident solar-simulated radiation. With the cut-off filter that removes 400 nm or shorter wavelengths, no photocatalytic behavior is observed, and the results resemble dark experiments only. The results indicate that the TiO_2 particles can be excited by the UV photons only, as will be further discussed in the Mechanism section.

For mineralization confirmation, values of TOC were measured for reaction mixture solutions before and after disinfection experiment completion. Further confirmation was also made by measuring the resulting amounts of nitrogen ions in the form of nitrate in the mixture after reaction completion.

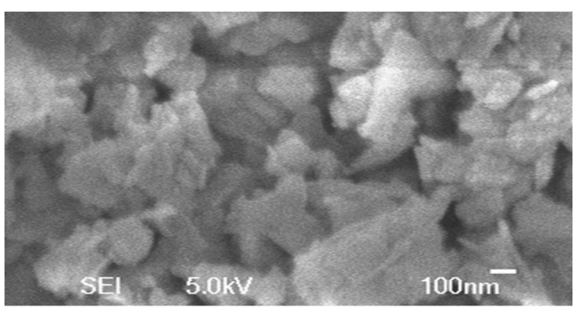

Fig. 2 SEM image of the solid commercial anatase TiO_2 powder.

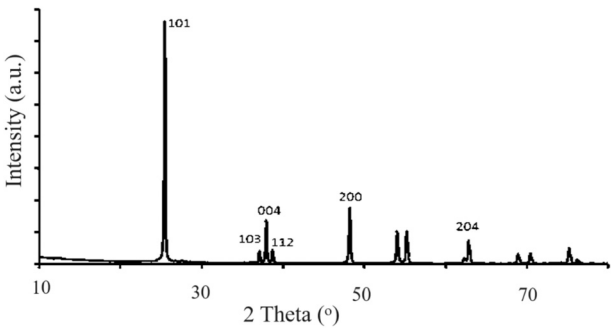

Fig. 3 XRD pattern of the TiO_2 powder.

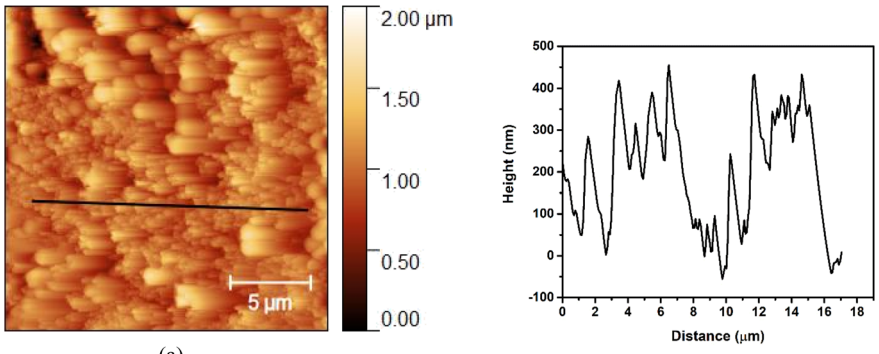

Fig. 4 AFM image of the TiO_2 film deposited on a glass surface: (a) surface analysis, and (b) height profiling.

Table 1 Efficiency values for powder anatase in bacterial deactivation. All experiments were conducted using 0.1 g of TiO_2 anatase in *S. aureus* (1×10^6 ± 5000 CFU mL^{-1} in 50 mL solution) at 25 ± 2 °C and pH 7.4 after 1 h under radiation intensity of 0.136 W cm^{-2}. Error = ±10%

Entry no.	Conditions	Lost bacteria (CFU) × 10^{-6}	Bacteria loss%	TN (lost CFU g^{-1} cat) × 10^{-6}	TF (TN min^{-1}) × 10^{-6}	QY[a] (lost bacteria per UV photon per g cat) × 10^{14}
1	No catalyst	—	0	—	—	—
2	Anatase, dark	9	18	90	1.5	—
3	Anatase, radiation	35	70	350	5.8	36.4
4	Anatase, radiation, filter	10	20	100	1.8	—

[a] Quantum yield calculations are described in Table S1.†

Control experiments were conducted under radiation with no catalysts. Other experiments involve bacterial solutions with catalysts in the dark. Photodegradation of the bacterial broth solutions was also examined. The results are shown with bacterial photodegradation results for comparison.

3.2.1. Powder catalyst. The powder TiO_2 readily catalyzes *S. aureus* inactivation under radiation. Table 1 shows differences in bacterial loss% values under various experimental conditions.

Table 1 shows that the powder anatase may induce *S. aureus* loss of ~70% in 1 h under radiation. With no catalyst, no bacterial loss can be observed. In the dark, only up to 18% loss is observed, which indicates the influence of the anatase on the bacteria, as described in the Introduction section above.

With longer exposure time, higher bacterial loss is observed, reaching ~80% in 3 h. To confirm mineralization of bacteria, the total organic carbon (TOC) was measured for the bacterial mixtures before and after exposure. Table 2 summarizes the measured TOC results.

Compared to the value in entry 4 (Table 2), the higher TOC value in entry 2 indicates bacterial growth under radiation with no catalyst. In the dark with catalyst (entry 3), no significant lowering in TOC can be observed. The values in entries 3 and 4 are similar within ±10% error. This means that no significant bacterial mineralization occurs. Therefore, the bacterial loss measured by counting in Table 1 is due to bacterial inactivation with no mineralization in the dark. On the other hand, the TOC value lowering in Table 2, entry 1, compared to entry 4, clearly indicates complete mineralization of bacteria. However, entry 1 still shows a higher organic content value than expected from the bacterial loss count. This is because the TOC values, measured for the gross reaction mixture after 3 h, include living bacteria, broth organics and cell walls from the mineralized bacteria. As reported earlier,[16,47] the *S. aureus* bacteria have thick walls which resist photodegradation. The TOC value is thus expected to increase.

Table 2, entry 5, also confirms the inability of the TiO_2 to induce mineralization in the presence of the cut-off filter. In such a case, only visible radiation reaches the catalyst. The TiO_2 particles are therefore not excited, and cannot induce mineralization for the bacteria or their organic content. Table 5 (entry 5) and Table 4 (entry 4) confirm the need for UV photons to induce photo-mineralization.

Table 2 TOC values measured for bacterial aqueous mixtures after 3 h. Experiments were performed using 0.1 g TiO_2 anatase against 50 mL solution of *S. aureus* (1×10^6 CFU mL^{-1}) in the dark and under a radiation intensity of 0.136 W cm^{-2} at 25 ± 2 °C and pH 7.4. TOC measurement error >10%

Entry no.	Conditions	TOC mg L^{-1}
1	TiO_2, radiation	26
2	No catalyst, radiation	46
3	TiO_2, dark	40
4	No catalyst, dark	42
5	TiO_2, radiation, filter	41

Table 3 Effect of *S. aureus* nominal concentration on the values of bacterial loss%, TN, TF and QY. Experiments performed using 0.1 g of TiO_2 powder anatase in 50 mL under a radiation intensity of 0.136 W cm^{-2} after 1 h at 25 ± 2 °C with stirring. Measurement error ±10%

Entry no.	Bacterial init. conc. (CFU mL^{-1}) × 10^{-6}	Lost bacteria (CFU) × 10^{-6}	Bacteria loss%	TN (lost bacteria per g cat) × 10^{-6}	TF (TN min^{-1}) × 10^{-6}	QY (lost bacteria per incident UV photon per g cat)
1	1	35.0	70	350	5.83	36.4×10^{-14}
2	3	93.0	62	930	15.50	97.0×10^{-14}
3	5	67.5	27	675	11.25	70.2×10^{-14}

Table 4 Effect of anatase loading on bacterial loss%, TN, TF and QY. Experiments conducted with stirring a 50 mL solution of *S. aureus* (1×10^6 CFU mL^{-1}) at 25 ± 2 °C and pH 7.4 under a radiation intensity of 0.136 W cm^{-2} for 1 h. Measurement error ±10%

Entry no.	Cat. loading (g)	Lost bacteria × 10^{-6}	Bacterial loss%	TN (lost bacteria per g cat) × 10^{-6}	TF (TN min^{-1}) × 10^{-6}	QY (lost bacteria per UV photon per g cat) × 10^{14}
1	1.500	32.5	65	21.6	0.4	2.3
2	0.100	35.0	70	350.0	5.8	36.4
3	0.050	20.0	40	395.0	6.6	41.1
4	0.025	14.0	28	560.0	9.3	58.3

Table 5 Recovery and reuse of the anatase powder catalyst. Experiments have been conducted with fresh (0.1 g), first-recovered and second-recovered anatase using 50 mL solutions of 1×10^6 CFU bacteria at pH 6.2 and 25 ± 2 °C under a radiation intensity of 0.136 W cm^{-2}. Error is 10%

Catalyst	Bacterial loss%	Recovered catalyst mass (g)	Lost bacteria CFU × 10^{-6}	TN (lost bacteria per g cat) × 10^{-6}
Fresh	100	0.100	100	500
1st recovery	32	0.035	16	475
2nd recovery	26	0.025	13	520

To further confirm bacterial mineralization, aliquots of bacterial mixtures were syringed out from the photocatalytic reaction mixtures after 3 h. The aliquots were filtered, and the clear filtrates were analyzed for nitrogen ions. Before reaction, at zero time, the NH_4^+ ion concentration is 10.3 mg L^{-1}, which is due to the dissolved broth materials. Ammonium accumulation in bacterial broth was previously reported in the literature.[48,49] After 3 h radiation, the NH_4^+ ion concentration increases to 17.1 mg L^{-1}. The difference indicates mineralization of bacteria during the photocatalytic reaction. These results further corroborate the conclusion that the inactivated bacteria are mineralized during the photocatalytic reactions.

The effect of the bacterial concentration on bacterial loss has been studied, as summarized in Table 3. The table shows a lower loss% with increased bacterial concentration (entries 1–3). However, the catalyst activity follows another trend. Entries 1 and 2 show higher bacterial loss, TN, TF and QY values, with increased initial bacterial concentration. This increase is justified by the increased probability of contact between the bacteria and the photo-excited catalyst particles with higher bacterial concentration. As the bacterial concentration is increased (entry 3), the catalyst activity decreases. This is due to the screening of the catalyst active sites by the high bacterial concentration. However, a comparison between entries 1 and 3 shows that the catalyst activity is still higher with higher bacterial concentration. The results indicate the practicality of using the TiO_2 nanoparticles in the removal of *S. aureus* from water even at higher concentrations.

The effect of the powder TiO_2 anatase catalyst loading on the bacterial removal has been studied (Table 4). The bacterial loss% increases with higher catalyst loading. However, entries 1–4 show that the catalyst efficiency, in terms of TN, TF and QY, decreases with higher catalyst loading. This is not unexpected. Typically, the higher catalyst loading yields higher loss% values due to a higher number of excited catalyst particles. However, with higher catalyst particle loading, the particles present at the reaction-mixture surface may screen the inner particles inside the reaction bulk from the incident photons. The relative efficiency thus

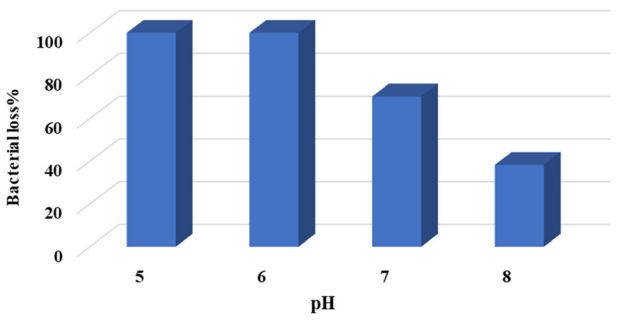

Fig. 5 Effect of pH value on *S. aureus* bacterial loss. Experiments conducted using 0.1 g TiO_2 powder, and 1×10^6 CFU mL^{-1} in 50 mL bacterial mixture at 25 ± 2 °C under a radiation intensity of 0.136 W cm^{-2}. Error is 10%.

decreases. This behavior indicates that using a powder catalyst has limitations.

The effect of the initial pH on bacterial loss under photocatalytic reaction conditions has been studied in acidic, neutral and basic media, as summarized in Fig. 5. Under the photocatalytic reaction conditions, the bacterial loss% decreases with increased nominal pH value. The reason is partly due to the value for the zero-charge point (P_{ZC}). P_{ZC} describes the pH value at which the solid surface carries a neutral charge.[50] For the TiO_2 surface, the P_{ZC} value is reported to be in the range of 6.5–7.5.[51,52] Therefore, in this range, the TiO_2 particle surface is neutral. Meanwhile, at lower pH, the surface is positively charged and it has negative charges at high pH. At a higher pH value, the negatively charged ZnO surface may repel the bacteria, which carries negative charges at their surfaces and keeps them away. This explains why the efficiency is low at high pH. The present results are contrary to other literature reports, where higher pH values are preferred in the photodegradation of Eriochrome Black T using Ni–P zeolite.[53] In that report, the zeolite showed a significant effect on the catalyst efficiency, which adds to the issue of the pH effect.

On the other hand, the *S. aureus* zeta potential is higher at lower pH, as described by Klodzinska *et al.*[54] At lower pH, the net surface charge decreases. Consequently, repulsions between bacteria decrease. Burel *et al.*[55] reported lowering in cellular negative-surface potential at lower pH and increased aggregation. Therefore, *S. aureus* bacteria have a greater tendency to aggregate at lower pH.[56] Their ability to adhere to surfaces also increases at lower pH.[57]

Thus, the higher bacterial loss at lower pH in Fig. 5 is due to the bacterial ability to get closer and adhere to solid surfaces like the catalyst. As such, the bacteria will be more affected by the photoexcited TiO_2 particle at lower pH value. However, for practical purposes, the pH value of 7.4 has been used here as a default value, unless otherwise stated. This value is within the pH range of 6.8–8.4 that is commonly encountered in natural surface waters.[58]

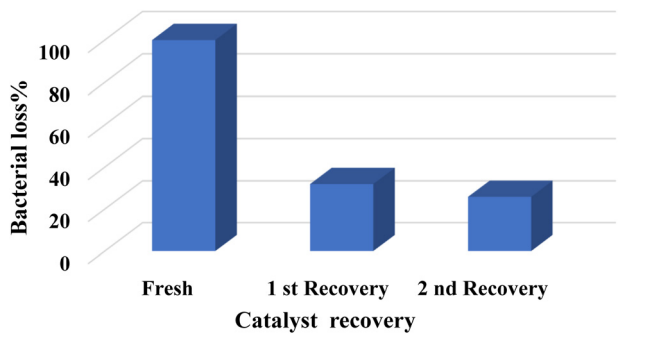

Fig. 6 Effect of powder catalyst recovery and reuse on *S. aureus* loss. Experiment conducted using fresh anatase TiO_2 (0.1 g), first recovered and second recovered catalyst. Fresh bacterial solution (50 mL, 1×10^6 CFU mL^{-1}) is used in each catalyst, with pH 6.2, for 1 h at 25 ± 2 °C under a radiation intensity of 0.136 W cm^{-2}. Error is 10%.

Powder catalyst recovery and reuse have been studied. Fig. 6 indicates that the bacterial loss% is reduced on catalyst recovery and reuse. While the fresh catalyst exhibits high bacterial loss%, the first-recovery catalyst shows only 32%, and the second-recovery catalyst shows only 26% value. This is expected from nanopowder photocatalyst systems. In fact, this is one limitation in using nanopowder photocatalysts in research. The small size of particles prevents efficient separation after reaction completion, as reported earlier.[59] Catalyst recovery has been made using simple decantation after reaction completion, which resulted in high catalyst loss during separation. Recalculating the date in Fig. 6 gives a better understanding. Up to two-thirds of the catalyst powder has been lost on first recovery. By calculating the catalyst efficiency in terms of TN, the results indicate a smaller loss in catalyst efficiency upon recovery due to lost catalyst mass during catalyst separation, as shown in Table 5.

3.2.2. Film catalyst. As described above, the TiO_2 powder catalyst exhibits soundly high efficiency in *S. aureus* inactivation and mineralization. However, it has limitations in larger scale water reclamation processes. Catalyst recovery and reuse are technically difficult, especially from bacterial suspensions. The suspended catalyst particles may also screen each other, which lowers the overall catalyst efficiency. Moreover, the suspended nanoparticle catalysts may not be used in larger scale water reclamation by continuous flow processes, as they may washed away with the continuous flow. For these reasons, the TiO_2 film catalyst has been prepared and examined, as described above.

Table 6 summarizes the values of bacterial loss after 3 h radiation experiments above film catalysts. By comparing the Table 6 results with those of Tables 1–4, the film catalyst exhibits much higher efficiency in removing *S. aureus*. The bacterial loss% is very different between the two systems. However, the relative efficiency per gram catalyst (expressed in TN, TF or QY values) is much higher for the film catalyst. The results corroborate the assumptions described above about the ability of the suspended particles to screen each other from incident photons.

Film catalyst recovery and reuse have been studied. The film catalyst has been recovered by simple methods with no technical difficulties. In order to avoid difficulties with bacterial growth during the fresh catalyst experiments (3 h), recovery and reuse, separate in-parallel control runs have been made. The recovered film catalyst has been used with a fresh bacterial solution, concurrently with a fresh catalyst in a separate experiment. Table 7 shows no significant loss in the film catalyst efficiency on recovery if the bacterial solutions are carefully managed. Therefore, bacterial solutions should not be left for long times under waiting conditions; otherwise, the recovery results may not be highly conclusive.

The nanopowder catalyst could not be assessed under continuous flow experiments. On the contrary, film catalysts have been used readily, as described in the Experimental section 2. For the continuous flow experiments, the film catalyst exhibits slightly higher efficiency than in the batch

Table 6 Effect of the TiO_2 film catalyst on *S. aureus* removal. Experiments conducted using two TiO_2 film slides (total TiO_2 mass ~2–3.2 × 10^{-3} g, total gross area 37.5 cm^2), in 100 mL bacterial solution (6.6 × 10^6 CFU mL^{-1}) at pH 7.4 and 25 ± 2 °C for 3 h under a radiation intensity of 0.136 W cm^{-2}. Measurement error ±10%

Entry	Conditions	Remaining bacteria concentration (CFU mL^{-1}) × 10^{-6}	Bacterial loss%	Lost bacteria (CFU) × 10^{-6}	TN (bacteria lost per g cat) × 10^{-9}	TF TN min^{-1} × 10^{-6}	QY (lost bacteria per UV photon per g cat) × 10^{12}
1	Dark, no catalyst	6.6	—	—	—	—	—
2	Dark, catalyst	6.3	4.5	30	4.6	25	—
3	Radiation, catalyst	1.4	79.0	521	81.4	2900	14

Table 7 Recovery and reuse of the anatase film catalyst. Experiments have been conducted using fresh, first-recovered and second-recovered anatase. Two TiO_2 slides (total TiO_2 mass ~2–3.2 × 10^{-3} g, total gross area 37.5 cm^2). pH 7.4, at 25 ± 2 °C, nominal bacterial solution ~6.5 × 10^6 CFU in 100 mL, for 3 h under a radiation intensity of 0.136 W cm^{-2}. Measurement error ±10%

Entry	Catalyst	Bacterial loss%	Lost bacteria (CFU) × 10^{-6}	TN (lost bacteria per g cat) × 10^{-9}	TF (TN min^{-1}) × 10^{-9}	QY (lost bacteria per UV photon per g cat) × 10^{-12}
3	Fresh	79	521	81	0.48	14.0
2	1st recovery	75	495	77	0.43	13.3
3	2nd recovery	76	501	78	0.43	13.5
4	Fresh cat[a]	75	495	77	0.43	13.3

[a] Fresh film catalyst used concurrently in parallel with the 1st recovered film catalyst as the control run.

Table 8 Comparison of the film catalyst efficiency between the batch and continuous flow processes. Experiments conducted using two fresh TiO_2 film catalysts (total TiO_2 mass ~2–3.2 × 10^{-3} g, total gross area 37.5 cm^2). Nominal bacterial solution ~6.5 × 10^6 CFU in 100 mL at pH 7.4 and 25 ± 2 °C for 3 h under a radiation intensity of 0.136 W cm^{-2}. Error is 10%

Description	Bacterial loss%	Lost bacteria (CFU) × 10^{-6}	TN (lost bacteria per g cat) × 10^{-9}	TF (TN min^{-1}) × 10^{-9}	QY (lost bacteria per UV photon per g cat) × 10^{-12}
Batch	79	521	81	0.49	14
Continuous	90	594	92	0.54	16

film catalytic experiments (Table 8). This is presumably due to the thinner solution mixture layer above the film catalyst used in the continuous flow process. Therefore, photon penetration to the catalyst film increases in the case of continuous flow.

3.3. Photocatalytic mechanism

Metal oxide nanoparticles are known to inactivate bacteria even in the dark.[60] The Gram+ *S. aureus* bacteria are no exception, and were inhibited by TiO_2 with no radiation.[61] In the dark, the bacteria are subjected to physical factors that cause their rupture; after which, the organic matter leaches out. However, under UV radiation, the process is more pronounced, as described here in Tables 1 and 2. Literature studies have also described the photocatalytic effect of TiO_2 under UV radiation on *S. aureus* bacteria inhibition.[62,63] As stated in section 1 here, previous literature studies described the inhibition and inactivation of the bacteria under photocatalytic conditions with the TiO_2 nanopowder together

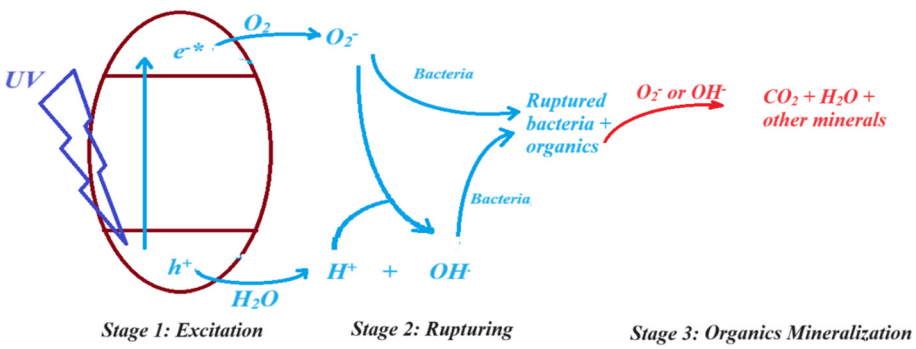

Fig. 7 Schematic showing a mechanism summary proposed for TiO_2 nanoparticles as a catalyst for the photo-degradation of aqueous bacteria, followed by their organic components. All stages are based on earlier literature.

with proposed mechanisms. Mechanistic pathways were also proposed for the photocatalytic mineralization of aqueous organic contaminants by TiO_2 (ref. 28 and 64) and other semiconducting materials.[65,66] In the present study, both processes readily occur. Therefore, based on the literature, earlier mechanisms have been used here, as described in Fig. 7. The adopted mechanism involves three stages:

1) First stage involves TiO_2 particle excitation. With a band gap of ~3.23 eV, the semiconductor TiO_2 nanoparticles can be excited by incident photons having enough energy (384 nm or shorter). Excited electrons (e^-*) move to the conduction band (CB), leaving holes (h^+) inside the valence band (CB). The e^-* have enough energy to reduce dissolved O_2 molecules and create superoxide (O_2^-) species that have high oxidizing power. The superoxide species may then oxidize various species in the medium. The bacterial cell walls are then ruptured by them. Alternatively, the superoxide species may react with water to create the highly reactive $OH^\bullet$ radicals, which may also oxidize various species. It should be noted that both O_2^- and $OH^\bullet$ species are short-lived reactive species (SLRS), and can function in the space close to the TiO_2 surface before being consumed. Such mechanisms were reported earlier,[28,67] and are not accredited to the present study.

2) Second stage involves the rupture of bacterial cell walls. The SLRS may rupture the bacterial wall. This occurs if the bacteria exist in close proximity to the excited TiO_2 particle. Once the bacterial cell walls are ruptured, the organic matter leaches out to the aqueous medium. While rupturing may still occur in the dark, it occurs more profoundly under irradiation, as stated above. Therefore, the influence of the radiation should be considered, and the main process is photocatalysis, as reported earlier.[61,68]

3) In the third stage, the organic stuff leaches out to the aqueous medium, either as soluble or as a suspension. In either case, the organic molecules are exposed to the excited TiO_2 particles and the short-lived reactive species. Therefore, the organic molecules are readily mineralized by the photocatalytic process. In this way, the organic molecules follow in a similar fashion, as reported for other organic contaminant molecules. TiO_2 nanoparticles are known to photo-catalyze the mineralization of aqueous organic contaminants, such as phenol derivatives,[69,70] chloro-hydrocarbons[70] and many others. Earlier proposed mechanisms have been adopted here.

The results in Tables 1 and 2 are justified by the earlier proposed mechanism. Photocatalysis may not occur in the dark or under visible light. With a wide band gap value of 3.23 eV, UV radiation of ~385 nm or shorter is needed to excite the catalyst particles, as described by earlier literature.[72,73] This justifies the results in Tables 1 and 2, where mineralization needs UV photons.

The mechanism explains the results observed here. The effect of pH on bacterial loss is justified. The bacterial inactivation is not pronounced under basic conditions here. This is simply because the TiO_2 surface is negatively charged and may thus repel the bacterial cell body, which also carries negative charges. In such a case, the bacteria are repelled from the TiO_2 particle, and are kept away from the SLRS. At pH values closer to their P_{ZC} value, the TiO_2 particle surfaces are neutral, which keeps the bacteria closer to the particle and the SLRS. At lower pH value, the bacteria may also agglomerate and adhere at the catalyst particle surfaces. This allows more exposure to the TiO_2 particles and the SLRS. More bacterial cell wall rupturing may thus occur. The optimal pH range for *S. aureus* growth is 7.0–7.5, but they can grow in a wider pH range of 4.2–9.3.[74,75]

The mechanism also explains how increasing bacteria concentration and powder catalyst loading increase bacterial loss%. However, at higher bacterial concentrations or catalyst loading, the catalytically active sites in the reaction mixture bulk are screened away from incident photons, which lowers the catalyst efficiency. Similarly, higher catalyst loading lowers the efficiency. This is clearly observed in the powder catalyst, where the surface particles screen the incident photons and lower the overall catalytic efficiency.

The higher efficiency exhibited by the film catalyst, compared to the powder catalyst, is explained by the mechanism. In film catalyst experiments, the reaction mixtures above the catalyst surface are used at relatively small heights. The reaction mixture only slightly screens the catalyst particles from the incident photons. In larger scale water disinfection processes, especially in cases of continuous flow, the maximum exposure of the catalyst films needs to be maintained.

Moreover, in film catalysts (both batch and continuous flow), the film thickness is too small at ~0.4 μm. Therefore, a good proportion of the catalyst particles are exposed to the incident photons, which increases the efficiency. Such behavior is more pronounced in the case of continuous flow experiments, where a smaller bacterial suspension depth is used.

The results show the feasibility of using TiO_2 nanoparticles as photocatalysts in the complete removal of bacteria. However, more research is needed in the area. Examining other types of nanoparticles (such as those of ZnO) is recommended. Using binary semiconductor systems, such as NiO–ZnO,[76] may increase the photocatalytic effect. Examining other binary photocatalyst systems with narrower band gaps, such as CdS–AgBr,[12,77] may improve the catalytic process in the visible region.

4. Conclusions

Anatase TiO_2 powder photocatalyzes *S. aureus* bacterial inactivation under solar-simulated radiations. Due to the TiO_2 wide band gap, the photocatalysis process is induced by the UV tail (5%) that exists in the incident radiations, as confirmed by cut-off filter control experiments. Total organic carbon and nitrate ion measurements confirm the mineralization of the bacteria and the broth under photodegradation conditions. Therefore, the process gives

prospects to remove the bacteria and their organic stuff through photodegradation. More bacteria are removed at lower pH value. At higher bacterial concentrations or TiO_2 powder loading, higher bacterial loss is observed, but the relative catalyst efficiency is lowered due to the screening of the catalyst sites. The relative efficiency (per g catalyst) is maintained on catalyst recovery and reuse, while catalyst mass loss occurs, which lowers the bacterial loss% on reuse. This is a technical difficulty that limits the powder catalysis process. Replacing the suspended powder TiO_2 catalyst with thin films improves the photocatalytic efficiency, and makes the catalyst recovery and removal easier and less costly. Film catalysts can also be employed in continuous flow experiments, while maintaining high efficiency.

Author contributions

Raed Shqier: investigation (powder catalysis). Ahed Zyoud: supervision. Muath H. S. Helal: methodology (film catalysis), validation (checking powder catalysis), writing – review & editing. Heba Nassar: methodology (catalyst film preparations, spectral analysis), editing. Raed Alkowni: project administration (bacterial culturing). Mohyeddin Assali: investigation (film characterization). Shaher Zyoud: investigation (TOC measurement). Naser Qamhieh: investigation (powder characterization). Abdul Razack Hajamohideen: investigation (powder characterization). Shadi Sawalha: investigation (film characterization). Samer H. Zyoud: investigation (powder characterization). Hikmat S. Hilal: supervision, project administration, writing – original draft.

Conflicts of interest

There are no conflicts to declare.

Acknowledgements

Assistance by the technical staff, An-Najah N. University, is acknowledged. The project received no special funding. Parts of the powder catalyst results are based on Raed Shqier MSc Thesis, An-Najah N. University.

References

1 M. Qiu, L. Liu, Q. Ling, Y. Cai, S. Yu, S. Wang, D. Fu, B. Hu and X. Wang, Biochar for the removal of contaminants from soil and water: a review, *BioChar*, 2022, **4**, 19.

2 M. N. Shiadeh, M. Sepidarkish, A. Mollalo, N. As' adi, S. Khani, Z. Shahhosseini, M. Danesh, S. Esfandyari, A. H. Mokdad and A. Rostami, Worldwide prevalence of maternal methicillin-resistant Staphylococcus aureus colonization: A systematic review and meta-analysis, *Microb. Pathog.*, 2022, 105743.

3 T. Azuma, M. Murakami, Y. Sonoda, A. Ozaki and T. Hayashi, Occurrence and Quantitative Microbial Risk Assessment of Methicillin-Resistant Staphylococcus aureus (MRSA) in a Sub-Catchment of the Yodo River Basin, Japan, *Antibiotics*, 2022, **11**, 1355.

4 A. Yousefi and A. Nezamzadeh-Ejhieh, Preparation and characterization of SnO2-BiVO4-CuO catalyst and kinetics of phenazopyridine photodegradation, Iranian, *J. Catal.*, 2021, **11**, 247–259.

5 M. Lindmark, K. Cherukumilli, Y. S. Crider, P. Marcenac, M. Lozier, L. Voth-Gaeddert, D. S. Lantagne, J. R. Mihelcic, Q. M. Zhang and C. Just, Passive In-Line Chlorination for Drinking Water Disinfection: A Critical Review, *Environ. Sci. Technol.*, 2022, **56**, 9164–9181.

6 T. Gao, H. Wang, J. Xu, C. Hu and L. Lyu, Enhanced Water Purification Efficiency Induced by Trace H2O2 on the Electron Distribution-Polarized Unequilibrium Surface of CuS/ZnO Nanosheets, *ACS ES&T Water*, 2022, **3**, 79–85.

7 J. Wang, H. Liu, Y. Wang, D. Ma, G. Yao, Q. Yue, B. Gao and X. Xu, A new UV source activates ozone for water treatment: Wavelength-dependent ultraviolet light-emitting diode (UV-LED), *Sep. Purif. Technol.*, 2022, **280**, 119934.

8 V. R. Moreira, Y. A. R. Lebron, L. V. de Souza Santos and M. C. S. Amaral, Low-cost recycled end-of-life reverse osmosis membranes for water treatment at the point-of-use, *J. Cleaner Prod.*, 2022, **362**, 132495.

9 E. T. Anthony, M. O. Ojemaye, A. I. Okoh and O. O. Okoh, Potentials of low-cost methods for the removal of antibiotic-resistant bacteria and their genes in low budget communities: A review, *J. Water Proc. Engineering*, 2021, **40**, 101919.

10 E. Detenchuk, D. Mazur, T. Latkin and A. Lebedev, Halogen substitution reactions of halobenzenes during water disinfection, *Chemosphere*, 2022, **295**, 133866.

11 R. Alabada, A. Ayub, Y. Ajaj, S. I. Bhat, R. H. Alshammari, A. Abduldayeva, A. I. Mallhi, Z. Ahmad and R. M. Mohamed, A new approach to the synthesis of CuMoO4 nanoparticles with mechanistic insight into the sunlight-assisted degradation of textile pollutants and antibacterial activity evaluation, *J. Alloys Compd.*, 2024, **977**, 173400.

12 S. A. Mirsalari, A. Nezamzadeh-Ejhieh and A. R. Massah, A designed experiment for CdS-AgBr photocatalyst toward methylene blue, *Environ. Sci. Pollut. Res.*, 2022, **29**, 33013–33032, DOI: **10.1007/s11356-021-17569-1**.

13 X. Jaramillo-Fierro and M. F. Cuenca, Novel Semiconductor Cu (C3H3N3S3) 3/ZnTiO3/TiO2 for the Photoinactivation of E. coli and S. aureus under Solar Light, *Nanomaterials*, 2023, **13**, 173.

14 W. Wang, G. Huang, C. Y. Jimmy and P. K. Wong, Advances in photocatalytic disinfection of bacteria: development of photocatalysts and mechanisms, *J. Environ. Sci.*, 2015, **34**, 232–247.

15 A. Zyoud, M. Dwikat, S. Al-Shakhshir, S. Ateeq, J. Shteiwi, A. Zu'bi, M. H. Helal, G. Campet, D. Park and H. Kwon, Natural dye-sensitized ZnO nano-particles as photo-catalysts in complete degradation of E. coli bacteria and their organic content, *J. Photochem. Photobiol., A*, 2016, **328**, 207–216.

16 A. H. Zyoud, M. Dwikat, S. Al-Shakhshir, S. Ateeq, J. Ishtaiwa, M. H. Helal, M. Kharoof, S. Alami, H. Kelani and

G. Campet, ZnO nanoparticles in complete photo-mineralization of aqueous gram negative bacteria and their organic content with direct solar light, *Sol. Energy Mater. Sol. Cells*, 2017, **168**, 30–37.

17 C. L. de Dicastillo, M. G. Correa, F. B. Martínez, C. Streitt and M. J. Galotto, Antimicrobial effect of titanium dioxide nanoparticles, *Antimicrobial Resistance-A One Health Perspective*, 2020.

18 A. Kubacka, M. S. Diez, D. Rojo, R. Bargiela, S. Ciordia, I. Zapico, J. P. Albar, C. Barbas, V. A. Martins dos Santos and M. Fernández-García, Understanding the antimicrobial mechanism of TiO2-based nanocomposite films in a pathogenic bacterium, *Sci. Rep.*, 2014, **4**, 4134.

19 H. Xu, B. Liu, W. Qi, M. Xu, X. Cui, J. Liu and Q. Li, Combined impact of TiO2 nanoparticles and antibiotics on the activity and bacterial community of partial nitrification system, *PLoS One*, 2021, **16**, e0259671.

20 J. Singh, P. B. Hegde, S. Avasthi and P. Sen, Scalable Hybrid Antibacterial Surfaces: TiO2 Nanoparticles with Black Silicon, *ACS Omega*, 2022, **7**, 7816–7824.

21 I. Levchuk, T. Homola, J. Moreno-Andrés, J. J. Rueda-Márquez, P. Dzik, M. Á. Morínigo, M. Sillanpää, M. A. Manzano and R. Vahala, Solar photocatalytic disinfection using ink-jet printed composite TiO2/SiO2 thin films on flexible substrate: Applicability to drinking and marine water, *Sol. Energy*, 2019, **191**, 518–529.

22 A. Sinha, J. Qian, S. L. Moffitt, K. Hurst, K. Terwilliger, D. C. Miller, L. T. Schelhas and P. Hacke, UV-induced degradation of high-efficiency silicon PV modules with different cell architectures, *Progr. Photovolt.: Res. Appl.*, 2023, **31**, 36–51.

23 B. P. Howden, S. G. Giulieri, T. Wong Fok Lung, S. L. Baines, L. K. Sharkey, J. Y. Lee, A. Hachani, I. R. Monk and T. P. Stinear, Staphylococcus aureus host interactions and adaptation, *Nat. Rev. Microbiol.*, 2023, 1–16.

24 M. Gatti, S. Barnini, F. Guarracino, E. M. Parisio, M. Spinicci, B. Viaggi, S. D'Arienzo, S. Forni, A. Galano and F. Gemmi, Orthopaedic implant-associated staphylococcal infections: a critical reappraisal of unmet clinical needs associated with the implementation of the best antibiotic choice, *Antibiotics*, 2022, **11**, 406.

25 B. M. Lund, T. C. Baird-Parker and G. W. Gould, *Microbiological safety and quality of food*, Springer Science & Business Media, 2000.

26 J. M. Jay, M. J. Loessner and D. A. Golden, *Modern food microbiology*, Springer Science & Business Media, 2008.

27 A. Ajmal, I. Majeed, R. Malik, H. Idriss and M. Nadeem, Principles and mechanisms of photocatalytic dye degradation on TiO2 based photocatalysts: a comparative overview, *RSC Adv.*, 2014, **4**, 37003–37026.

28 H. M. El Sharkawy, A. M. Shawky, R. Elshypany and H. Selim, Efficient photocatalytic degradation of organic pollutants over TiO2 nanoparticles modified with nitrogen and MoS2 under visible light irradiation, *Sci. Rep.*, 2023, **13**, 8845.

29 Y. Cardona, A. Węgrzyn, P. Miśkowiec, S. A. Korili and A. Gil, Catalytic photodegradation of organic compounds using TiO2/pillared clays synthesized using a nonconventional aluminum source, *Chem. Eng. J.*, 2022, **446**, 136908.

30 D. K. Muthee and B. F. Dejene, Effect of annealing temperature on structural, optical, and photocatalytic properties of titanium dioxide nanoparticles, *Heliyon*, 2021, **7**, e07269.

31 A. Taherniya and D. Raoufi, The annealing temperature dependence of anatase TiO2 thin films prepared by the electron-beam evaporation method, *Semicond. Sci. Technol.*, 2016, **31**, 125012.

32 X. Chen, S. N. Hosseini and M. A. van Huis, Heating-induced transformation of anatase TiO2 nanorods into rock-salt TiO nanoparticles: implications for photocatalytic and gas-sensing applications, *ACS Appl. Nano Mater.*, 2022, **5**, 1600–1606.

33 M. Frobisher, *Fundamentals of microbiology*, WB Saunders Company, Philadelphia, 6th edn, 1957.

34 S. El-Kacemi, H. Zazou, N. Oturan, M. Dietze, M. Hamdani, M. Es-Souni and M. A. Oturan, Nanostructured ZnO-TiO 2 thin film oxide as anode material in electrooxidation of organic pollutants. Application to the removal of dye Amido black 10B from water, *Environ. Sci. Pollut. Res.*, 2017, **24**, 1442–1449.

35 W. E. Federation, *Association APH, Standard methods for the examination of water and wastewater*, American Public Health Association (APHA), Washington, DC, USA, 2005.

36 H. Nassar, A. Zyoud, H. H. Helal, H. Ghannam, T. W. Kim, M. H. Helal and H. S. Hilal, Fluorine tin oxide-supported copper nanofilms as effective and selective de-nitration electrocatalysts, *J. Electroanal. Chem.*, 2022, **911**, 116249.

37 R. M. Pashley and M. E. Karaman, *Applied colloid and surface chemistry*, John Wiley & Sons, 2021.

38 S. Glasstone and D. Lewis, *Elements of physical chemistry*, D. Van Nostrand Co., NY, 1960.

39 R. Brüninghoff, K. Wenderich, J. P. Korterik, B. T. Mei, G. Mul and A. Huijser, Time-dependent photoluminescence of nanostructured anatase TiO2 and the role of bulk and surface processes, *J. Phys. Chem. C*, 2019, **123**, 26653–26661.

40 L. Kernazhitsky, V. Shymanovska, T. Gavrilko, V. Naumov, L. Fedorenko, V. Kshnyakin and J. Baran, Laser-excited excitonic luminescence of nanocrystalline TiO2 powder, *Ukr. J. Phys.*, 2014, **59**, 248–255.

41 T. Luttrell, S. Halpegamage, J. Tao, A. Kramer, E. Sutter and M. Batzill, Why is anatase a better photocatalyst than rutile?-Model studies on epitaxial TiO2 films, *Sci. Rep.*, 2014, **4**, 4043.

42 N. Mehrabanpour, A. Nezamzadeh-Ejhieh, S. Ghattavi and A. Ershadi, A magnetically separable clinoptilolite supported CdS-PbS photocatalyst: Characterization and photocatalytic activity toward cefotaxime, *Appl. Surf. Sci.*, 2023, **614**, 156252.

43 F. Soori and A. Nezamzadeh-Ejhieh, Synergistic effects of copper oxide-zeolite nanoparticles composite on photocatalytic degradation of 2, 6-dimethylphenol aqueous solution, *J. Mol. Liq.*, 2018, **255**, 250–256.

44 S. Vahabirad, A. Nezamzadeh-Ejhieh and M. Mirmohammadi, A co-precipitation synthesized BiOI/(BiO)

2CO3 nanocatalyst: An experimental design and mechanism study towards photodegradation of sulfasalazine, *J. Taiwan Inst. Chem. Eng.*, 2023, **151**, 105139.
45 F. Scarpelli, T. F. Mastropietro, T. Poerio and N. Godbert, Mesoporous TiO2 thin films: State of the art, *Titanium Dioxide-Material for a Sustainable Environment*, 2018, vol. 508, pp. 135–142.
46 H. Zabihi-Mobarakeh and A. Nezamzadeh-Ejhieh, Application of supported TiO2 onto Iranian clinoptilolite nanoparticles in the photodegradation of mixture of aniline and 2, 4-dinitroaniline aqueous solution, *J. Ind. Eng. Chem.*, 2015, **26**, 315–321.
47 A. Zyoud, R. Alkowni, O. Yousef, M. Salman, S. Hamdan, M. H. Helal, S. F. Jaber and H. S. Hilal, Solar light-driven complete mineralization of aqueous gram-positive and gram-negative bacteria with ZnO photocatalyst, *Sol. Energy*, 2019, **180**, 351–359.
48 K. Iwata, A. Azlan, H. Yamakawa and T. Omori, Ammonia accumulation in culture broth by the novel nitrogen-fixing bacterium, Lysobacter sp. E4, *J. Biosci. Bioeng.*, 2010, **110**, 415–418.
49 X. Yang, Y. Jiang, S. Wang, R. Zou, Y. Su, I. Angelidaki and Y. Zhang, Self-sustained ammonium recovery from wastewater and upcycling for hydrogen-oxidizing bacteria-based power-to-protein conversion, *Bioresour. Technol.*, 2022, **344**, 126271.
50 F. Soleimani and A. Nezamzadeh-Ejhieh, Study of the photocatalytic activity of CdS–ZnS nano-composite in the photodegradation of rifampin in aqueous solution, *J. Mater. Res. Technol.*, 2020, **9**, 16237–16251.
51 A. H. Zyoud, A. Zubi, S. Hejjawi, S. H. Zyoud, M. H. Helal, S. H. Zyoud, N. Qamhieh, A. Hajamohideen and H. S. Hilal, Removal of acetaminophen from water by simulated solar light photodegradation with ZnO and TiO2 nanoparticles: Catalytic efficiency assessment for future prospects, *J. Environ. Chem. Eng.*, 2020, **8**, 104038.
52 M. Zeng, Influence of TiO 2 surface properties on water pollution treatment and photocatalytic activity, *Bull. Korean Chem. Soc.*, 2013, **34**, 953–956.
53 A. N. Ejhieh and M. Khorsandi, Photodecolorization of Eriochrome Black T using NiS–P zeolite as a heterogeneous catalyst, *J. Hazard. Mater.*, 2010, **176**, 629–637.
54 E. Klodzinska, M. Szumski, E. Dziubakiewicz, K. Hrynkiewicz, E. Skwarek, W. Janusz and B. Buszewski, Effect of zeta potential value on bacterial behavior during electrophoretic separation, *Electrophoresis*, 2010, **31**, 1590–1596.
55 C. Burel, R. Dreyfus and L. Purevdorj-Gage, Physical mechanisms driving the reversible aggregation of Staphylococcus aureus and response to antimicrobials, *Sci. Rep.*, 2021, **11**, 15048.
56 L. Fernández Llamas, D. Gutiérrez, M. P. García Suárez and A. Rodríguez González, Environmental pH is a key modulator of Staphylococcus aureus biofilm development under predation by the virulent phage phiIPLA-RODI, *ISME J.*, 2021, **15**, 245–259.
57 F. Hamadi, H. Latrache, M. Mabrrouki, A. Elghmari, A. Outzourhit, M. Ellouali and A. Chtaini, Effect of pH on distribution and adhesion of Staphylococcus aureus to glass, *J. Adhes. Sci. Technol.*, 2005, **19**, 73–85.
58 L.-Q. Jiang, B. R. Carter, R. A. Feely, S. K. Lauvset and A. Olsen, Surface ocean pH and buffer capacity: past, present and future, *Sci. Rep.*, 2019, **9**, 18624.
59 T. Zorba, H. Nassar, M. H. Helal, J. Song, T. W. Kim, S. Jodeh and H. S. Hilal, Perovskite Nano-Powder and Nano-Film Catalysts in Mineralization of Aqueous Organic Contaminants through Solar Simulated Radiation, *Processes*, 2023, **11**, 2378.
60 L. Lifen, B. John and K. L. Yeung, Non-UV germicidal activity of fresh TiO2 and Ag/TiO2, *J. Environ. Sci.*, 2009, **21**, 700–706.
61 X. Jiang, B. Lv, Y. Wang, Q. Shen and X. Wang, Bactericidal mechanisms and effector targets of TiO2 and Ag-TiO2 against Staphylococcus aureus, *J. Med. Microbiol.*, 2017, **66**, 440.
62 L. Çobani and A. M. Valentine, Microbial interactions with titanium, in *Microbial metabolism of metals and metalloids*, Springer, 2022, pp. 527–543.
63 A. B. Younis, V. Milosavljevic, T. Fialova, K. Smerkova, H. Michalkova, P. Svec, P. Antal, P. Kopel, V. Adam and L. Zurek, Synthesis and characterization of TiO2 nanoparticles combined with geraniol and their synergistic antibacterial activity, *BMC Microbiol.*, 2023, **23**, 207.
64 H. Zhou, H. Wang, C. Yue, L. He, H. Li, H. Zhang, S. Yang and T. Ma, Photocatalytic degradation by TiO2-conjugated/coordination polymer heterojunction: Preparation, mechanisms, and prospects, *Appl. Catal., B*, 2023, 123605.
65 S. Ghattavi and A. Nezamzadeh-Ejhieh, A visible light driven AgBr/g-C3N4 photocatalyst composite in methyl orange photodegradation: focus on photoluminescence, mole ratio, synthesis method of g-C3N4 and scavengers, *Composites, Part B*, 2020, **183**, 107712.
66 M. Rezaei and A. Nezamzadeh-Ejhieha, The ZnO-NiO nano-composite: a brief characterization, kinetic and thermodynamic study and study the Arrhenius model on the sulfasalazine photodegradation, *Int. J. Hydrogen Energy*, 2020, **45**, 24749–24764.
67 G. Sujatha, S. Shanthakumar and F. Chiampo, UV light-irradiated photocatalytic degradation of coffee processing wastewater using TiO2 as a catalyst, *Environments*, 2020, **7**, 47.
68 E. Kanata, I. Paspaltsis, S. Sotiriadis, C. Berberidou, S. Tsoumachidou, D. Dafou, K. Xanthopoulos, M. Arsenakis, A. Arsenakis and I. Poulios, Photo-Fenton and TiO2 Photocatalytic Inactivation of Model Microorganisms under UV-A; Comparative Efficacy and Optimization, *Molecules*, 2023, **28**, 1199.
69 G. Keerthiga, K. Avinash, R. Saha, A. Balakrishnan and I. Jain, Photocatalytic degradation of nitro phenol: A continuous study in a TiO2 film coated photo reactor, *AIP Conf. Proc.*, 2023, **2427**, 020075.
70 I. Rangel-Vázquez, G. Del Angel, E. Ramos-Ramírez, F. González, P. Acevedo-Peña, C. M. Gómez, F. Tzompantzi, N. Gutiérrez-Ortega and J. Torres-Torres, Improvement of photocatalytic activity in the degradation of 4-chlorophenol

and phenol in aqueous medium using tin-modified TiO 2 photocatalysts, *RSC Adv.*, 2023, **13**, 13862–13879.

71 Z. M. Moushumy, M. J. Hassan, M. Ahsan, M. M. Hasan, M. N. Uddin, Y. Nagao and M. A. Hasnat, Photocatalytic degradation of chlorazol yellow dye under sunlight irradiation using Ce, Bi, and N co-doped TiO2 photocatalyst in neutral medium, *Environ. Sci. Pollut. Res.*, 2023, **30**, 35153–35169.

72 M. Khalafi, A. Nikfarjam, H. Hajghassem and S.-. Bidmeshkipour, UV activated single aligned TiO2 nanofiber embedded silver nanoparticles as room temperature ammonia gas sensor, *Phys. Scr.*, 2023, 085930.

73 R. Ghamarpoor, A. Fallah and M. Jamshidi, Investigating the use of titanium dioxide (TiO2) nanoparticles on the amount of protection against UV irradiation, *Sci. Rep.*, 2023, **13**, 9793.

74 J. Hudson, *Microbiological safety of meat|Staphylococcus aureus*, 2022.

75 X. Liao, X. Chen, A. S. Sant'Ana, J. Feng and T. Ding, Pre-Exposure of Foodborne Staphylococcus aureus Isolates to Organic Acids Induces Cross-Adaptation to Mild Heat, *Microbiol. Spectrum*, 2023, **11**, e0383222.

76 H. Derikvandi and A. Nezamzadeh-Ejhieh, Increased photocatalytic activity of NiO and ZnO in photodegradation of a model drug aqueous solution: effect of coupling, supporting, particles size and calcination temperature, *J. Hazard. Mater.*, 2017, **321**, 629–638.

77 S. A. Mirsalari and A. Nezamzadeh-Ejhieh, Focus on the photocatalytic pathway of the CdS-AgBr nano-catalyst by using the scavenging agents, *Sep. Purif. Technol.*, 2020, **250**, 117235.